Classification: Biological Science – Ecology,

Title: Host and parasite thermal ecology jointly determine the effect of climate warming on epidemic dynamics

Authors: Alyssa-Lois M. Gehman[1†*], Richard J. Hall[1,2,3] and James E. Byers[1,3]

Affiliations:

[1]Odum School of Ecology, University of Georgia, 140 E. Green St., Athens, GA 30602.

[2]Department of Infectious Diseases, College of Veterinary Medicine, University of Georgia, 501 D.W. Brooks Dr., Athens GA 30602

[3]Center for the Ecology of Infectious Diseases, University of Georgia, 140 E. Green St., Athens, GA, 30602

*Correspondence to: Alyssa-Lois M. Gehman
alyssamina@gmail.com

†Current address: Zoology, University of British Columbia, 6270 University Blvd., Vancouver, BC, V6T 1Z4

Keywords: disease ecology, thermal performance curves, marine ecology, epidemiological modeling, rhizocephalans

Supplemental Information:

Materials and Methods

A. Study System

Eurypanopeus depressus is an abundant oyster reef-dwelling crab occurring from the Gulf of Mexico to Massachusetts Bay. Temperature varies considerably across this range, and within individual sites seasonally. Refuge within the oyster reef ameliorates desiccation stress and protects *E. depressus* from predation (1, 2). Although there is a great range of oyster reef size and shape, the average reef found near Savannah, GA is ~200m^2, and average density of *E. depressus* is 120 adult m^{-2} (4-20mm carapace width; 3).

The mean expected longevity of adult *E. depressus* (from their first larval release) is 2.2 years, with a maximum life span of 3.5 years (4). Female *E. depressus* reproduction varies from south to north, with ovigerous females found year-round in south Florida (5), and between July and October in Delaware (6). *Eurypanopeus depressus* has 4 zoeal stages and one megalopal stage (under laboratory conditions; 7), and larvae take approximately 40 days to develop into the first crab stage (8). Host larval behavior suggests that *E. depressus* recruitment is retained within estuaries, with larvae migrating towards the surface during flood tide and towards the bottom at ebb tide (9, 10). Although recruitment is likely relatively closed between estuaries, crab larvae within an estuary are likely mixed, meaning a crab assemblage on a given oyster reef (the scale of our model) is likely experiencing open recruitment from crabs on other oyster reefs within the estuary.

Loxothylacus panopaei is a castrating rhizocephalan barnacle parasite that infects the mud crab *E. depressus*, as well as several other mud crabs (*13*,*33*). *Loxothylacus panopaei* is native to the Gulf of Mexico and introduced to the US Atlantic coast from Long Island, New York to Cape Canaveral, Florida. Genetic work suggests that there are three lineages of this parasite in its native range, and only the ER lineage is invasive along the US Atlantic coast (11). *Eurypanopeus depressus* is infected by the ER lineage, which was first documented in North Carolina in 1983 and in Georgia and northeastern Florida in 2004/2005 (12, 13). The Harris mud crab *Rithropanopeus harrisi* is also infected by the ER lineage, and could serve as a reservoir host for this parasite; however, it is generally found in lower salinities than are documented where this study took place (3). Although *L. panopaei* is present within the Gulf of Mexico and in Northern Florida, it has not been reported in southeastern Florida, suggesting that the higher temperatures in southeastern Florida may represent poor conditions for the parasite and be limiting spread (11). At a local level, there is evidence that temperature may drive seasonal patterns in parasite infection, with infection prevalence increasing in the spring, followed by a marked decrease in infection prevalence mid-summer, correlated with temperatures reaching above 25°C (14). Together these observations suggest that temperature may be driving changes *L. panopaei* infection prevalence.

Rhizocephalans have direct transmission, and the adult parasite resides within its crab host and produces larvae, lending itself for quantification of reproductive output. *Loxothylacus panopaei* larvae are planktonic and lecithotrophic (non-feeding), take 2-5 days to become infectious and can be male or female (Fig. S1 A, B, C and F; 15, 16). The sexes have very different roles within the transmission cycle; female larvae find and infect susceptible hosts, form an internal infection (interna) and subsequently release a virgin externa (Fig. S1 C, D, and E; 17). Exposed hosts are infected, but non-reproductive and the time to release of the virgin

externa can take from 18-57 days (Fig. S1 D and E; 18). For the parasite to become reproductive, and thus infectious, a male larva must recruit to the virgin externa after which the ovary develops to reproductive maturity (Fig. S1 F and G; 19). The time between a male larva colonizing a virgin externa and the parasite reaching reproductive maturity can take from 18-22 days (Fig. S1 G and H; 18). Parasite reproductive output is dependent on host size, with negligible reproductive output in hosts smaller then 8mm carapace width (20), and infection is rarely found in crabs less then 6mm carapace width (3).

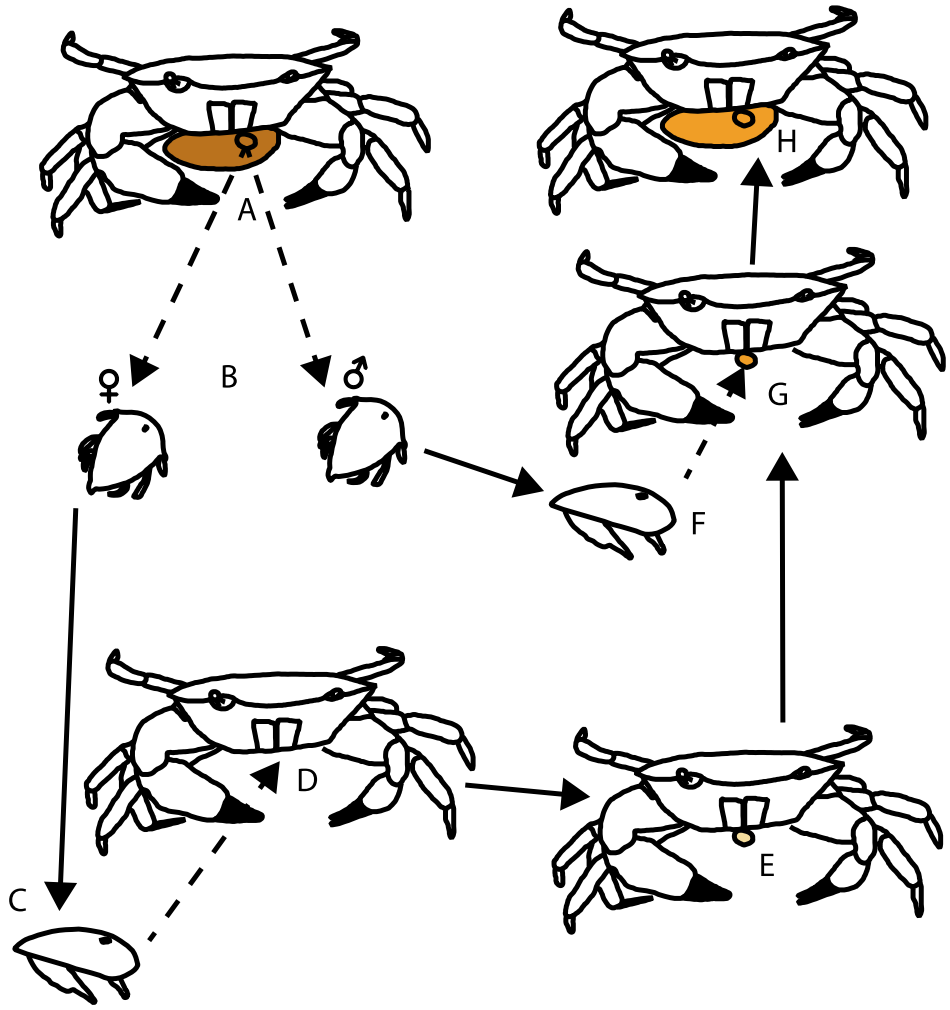

Figure S1. The simplified life-cycle of *Loxothylacus panpaei* adapted from (17). Dashed lines indicate migration and the solid lines indicate developmental changes. A mature externa on a *Eurypanopeus depressus* (A) releases free-living male and female nauplii (B). The female nauplii matures into a cyprid (C) which recruits to a susceptible host (D). Within the exposed host the female *L. panopaei* develops internal and external structures, releasing a virgin externa (E). The male nauplii matures into a cyprid (F) which recruits to a virgin externa (G) and upon internal fertilization the externa will then mature (H) and begin to produce parasite larvae (A). Barnacle larval stages (B, C, and F) are not drawn to scale; they are greatly enlarged for visibility.

B. Experimental

i. Seasonal Surveys: To evaluate parasite prevalence across seasons, we established 5 permanent monitoring sites along Romerly Marsh, Georgia (3, 21, 22). From 2010-2012, we placed a single 0.25 m^2 quadrat mid-reef on each reef. All oysters, dead shell and sediments to a depth of 10 cm were excavated from inside each quadrat. Samples were brought back to the lab, rinsed and sieved with a 1 mm mesh, and all infauna (i.e., invertebrates that live within the oyster reef) were placed in 10% formaldehyde for storage. All mud crabs were identified to species and examined for an externa. To constrain our estimate of infection probability to infectious individuals, we only counted *L. panopaei* infections that were developed to reproductive maturity (i.e., we did not count crabs with virgin externa or that were in the initial, internal-only stage of infection). From 2013-2014 oyster clumps were collected haphazardly by hand from near one of the five established reefs in Romerly Marsh, GA. Clumps were brought back to the lab, rinsed and sieved with a 1 mm mesh, and *E. depressus* were immediately removed and examined for externa.

ii. Lab experiment: To create thermal performance curves for multiple stages of parasite infection, we collected crabs from Romerly Marsh Creek, Savannah, GA (31°55'15.5"N 80°59'13.0"W) from 9 March to 23 April 2014. Because age of infection could affect parasite reproduction, we collected a single cohort of infected individuals to standardize infection age (i.e. we controlled time since externa release). Our own observations of this system suggested that in Georgia there is semi-synchronized release of virgin externa correlated with the seasonal increase in ambient water temperature above ~20°C (Fig. S2). To collect a cohort of approximately the same age *L. panopaei* infections and similar parasite reproductive potential, we isolated crabs not exhibiting external infections, controlling for host size (7.65-13.8mm in carapace width). We held crabs at ambient temperature, fed them frozen brine shrimp ad libitum and monitored for evidence of externa release. New infections, crabs exhibiting virgin externa, were first detected on 24 April 2014, and we began the exposed and infected class experiment (experiment A) on 13 May 2014*;* thus all infections were less than a month old at the start of the experiment (Fig. S2).

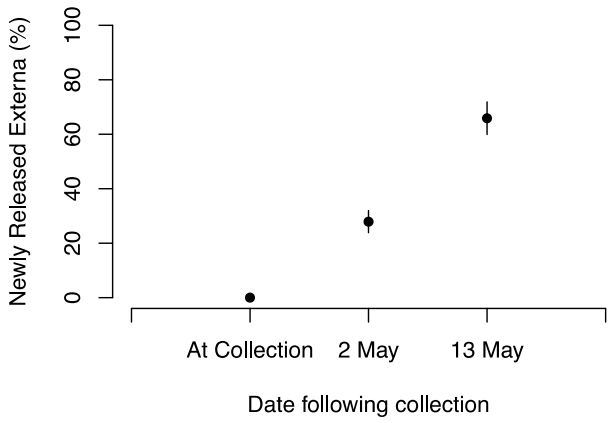

Figure S2. The percentage of newly released externa (+/- SE) from initially visibly uninfected crabs (N.B., these infections ostensibly stem from crabs that were internally infected upon collection). Crabs were collected between 9 March and 26 Apr 2014 and held in the lab. The first detection of a new externa release was found on 24 Apr 2014, and we began experiment A on 13 May 2014.

Spring is an ideal season to collect multiple stages of *L. panopaei* infection within their crab host. However, because internal infections have no visible externa it can be difficult to distinguish internal infections from uninfected crabs. Some life history traits can help to differentiate uninfected crabs. Specifically, *L. panopaei* causes complete sterilization, so if a female is ovigerous it is not currently infected (18, 19). In addition, *L. panopaei* feminizes its host, so *E. depressus* that have strong morphologically male traits are less likely to be infected. To take advantage of these traits and increase the chances of collecting uninfected hosts, we collected ovigerous females and male *E. depressus* for the susceptible class (uninfected). To minimize the risk of internal infection, we avoided collecting susceptible crabs during the spring when internal infection is more likely. Instead, we collected susceptible crabs from 3 July to 4 September 2014, and we maintained the crabs in filtered seawater in individual jars at ambient temperature and monitored for any evidence of infection. A few males exhibited virgin externa and were excluded, but no formerly ovigerous females ever exhibited externa. The susceptible experiment (experiment B) started on 28 September 2014.

Our objective for this study was to evaluate the effect of temperature on host-parasite survival and parasite reproduction by creating thermal performance curves for the infected, exposed and susceptible host. To achieve this goal, we ran two experiments, A and B. We subjected A) two stages of infected hosts—*E* (exposed, i.e., hosts with non-reproductive parasite stages), and *I* (infectious, i.e., hosts with the reproductively mature parasite stage) and B) *S*, uninfected hosts, to a range of temperatures that encompass the full range experienced in the field (Fig. 3A). For experiment A, seven coolers (Igloo 45L, 65 x 36 x 26 cm) were set up in a light and temperature controlled room, with ambient air temperature set to 15.5° C and a 12:12 light-cycle (8am to 8pm). We maintained each cooler as a water bath with a pump to keep water temperature consistent and well mixed. To keep crabs isolated but at the same temperature we placed 25 glass jars (30 mL spice jars, 56.6mm diameter, Freund 5023B06-B) within each cooler, on a porous shelf 130mm above the bottom of the cooler (Fig. S3). We kept crabs in 30μm-filtered seawater to ensure no parasite larvae could enter from the outside during the experiment, and thus we could maintain the non-mated state of the exposed infected crabs (individuals with virgin externa), and ensure that all observed parasite reproduction was produced by the experimental crabs. Water was changed every other day from 13 May to 24 June 2014, every four days from 24 June to 12 December 2014 and once a week from 12 December 2014 to 11 March 2015. To maintain the oxygen availability, each jar was fit with an air stone connected to an aerator.

Figure S3. Experimental setup for a single temperature treatment, with 20 jars each containing an *E. depressus*, fit with an airstone connected to an aerator. To maintain a constant temperature for the whole cooler we placed a single pump head next to an aquarium heater.

To calculate a thermal response curve for host-parasite survival and parasite reproduction rates we maintained cooler temperature treatments at targeted 5°C intervals from 5-35°C (Table S1), with one cooler for each temperature. We used chillers (RTE-111 and RTE-140) to cool water for the 5° and 10° C treatments. The 15ºC cooler was kept at ambient room temperature which was climate controlled at 15ºC. We used a single aquarium heater (Marine land submersible heater, 25W) to heat the 20° and 25°C treatments and two aquarium heaters for the 30° and 35°C treatments. To monitor the temperature treatments, we placed an ibutton into a single jar in each cooler with a temperature measurement every 10 minutes, and took the temperatures once daily with a hydrolab. To keep temperature constant in each jar during water changes we used aquarium heaters to raise filtered seawater to the exact temperature of the water bath before adding it into the crab jars in each treatment. Water changes were conducted one at a time, so that crabs were only outside of their temperature treatments for ~1 minute for each water change. To control for any effect of processing order we randomized the order in which water was changed for each water change.

Table S1. Average temperature and standard deviation for each cooler over the length of the experiment.

Experiment	Infection status	Temperature (ºC)	SD (ºC)
A	Exposed & Infected	5	0.13
A	Exposed & Infected	10	0.17
A	Exposed & Infected	15	0.85
A	Exposed & Infected	20	0.59
A	Exposed & Infected	26	0.48
A	Exposed & Infected	30	0.55
A	Exposed & Infected	36	1.27
B	Susceptible	5	0.07
B	Susceptible	14	0.62
B	Susceptible	20	0.59
B	Susceptible	30	0.27
B	Susceptible	34	2.09

The exposed and infected survival experiment (A; Table S1) ran for 312 days (including 11 days of acclimation). We randomly distributed 19-21 infected crabs into each of the seven temperature treatments, with 13-14 crabs with mature infections (infected) per treatment, and 6-7 crabs with virgin externa (exposed) per temperature. Because size has an effect on parasite reproduction we measured the carapace width and limited the range of included crabs to 7.65-13.8mm mm carapace width. We verified that crabs of different carapace width had been randomly distributed between the treatments (Fig. S4).

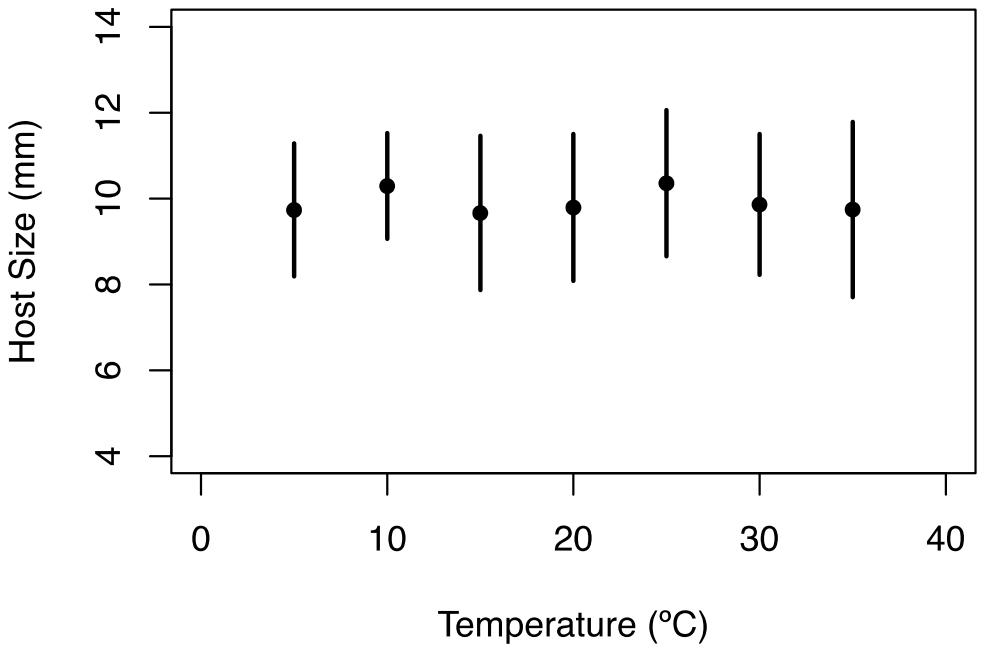

Figure S4. The mean and SD of host size (carapace width) for each of the temperature treatments.

The ambient water temperature at the beginning of the experiment was ~20º C and we started all temperature treatments at that temperature. We acclimated the *E. depressus* to their experimental treatments over the following 10 days, adjusting temperatures by 2°C per day until the target temperature was reached. The 2ºC temperature change was gradual, as we changed the setting of the water bath and let the bath slowly increase to the new temperature. Water changes were conducted every other day throughout the acclimation period. We only analyzed results starting after the acclimation period, when all crabs had been at experimental temperature for a full day (day 11, 25 May 2014).

For the susceptible *E. depressus* experiment (B; Table S1) we used fewer temperature treatments, but still captured the limits of the thermal curve. An additional five coolers were set up and crabs were acclimated as described above for the exposed and infected experiment, except that ambient water temperature was closer to 25ºC, and acclimation was done from that temperature. At each monitoring point, we checked for crab mortality and any evidence of infection. We did not find evidence of infection for any individual included in the susceptible category. Experiment B ran for 169 days (including 11 days of acclimation time).

For both experiment A and B, we monitored crabs at each water change. At each monitoring, we checked for crab and parasite mortality and parasite larval release. Nauplii and cyprid larval stages are visible to the naked eye, and we tested our detection limit by aliquoting known numbers of nauplii into jars and conducting two blind tests. In these trials, we readily detected nauplii concentrations down to 5 per jar, which is well within the error of our larval quantification and a tiny fraction of the larval concentrations typically produced by a reproductive parasite. In jars where we detected a release, or we were not confident of lack of release, we collected all contents of the jar by pouring out the water through a 30 μm mesh, then refilling the jar and again filtering the water through the mesh. Crabs remained within their jars throughout water changes. We then rinsed the contents on the mesh into a scintillation vial with ~15mL of 90% ethanol and stored for later quantification. If no release was detected, then the water was discarded and replaced. After water changes we fed the *E. depressus* the equivalent of one brine shrimp per day, placed within the experimental jars.

We quantified the number of larvae released using a gridded sedgewick rafter slide (model# 1801-G20). We homogenized samples by shaking them by hand, collected 1mL of sample and placed it into the counting chamber. We quantified all larvae present (cyprids, nauplii and eggs). We quantified the remaining volume of the sample in a graduated cylinder. Total number of larvae released was calculated by multiplying the number of larvae calculated in 1mL by the total volume of the sample (~15mL).

iii. Analysis*:* To quantify the effect of temperature on survival for each of the treatments we conducted survival analyses across temperature for the susceptible (uninfected), exposed (virgin externa) and infected *E. depressus*. We evaluated each infection status category individually using Kaplan-Meier survival analysis with the R package *survival*. This and all subsequent analyses and simulations were conducted using R 3.3.1 (23). We calculated the restricted mean survival time (RMST) at each temperature, which allowed us to estimate the expected weekly survival (i.e., lifespan) across treatments, even if experiments were not run for an equal length (24). We calculated RMST by estimating the area under the curve up to time t*, which we set to 52 weeks, allowing us to evaluate the expected lifespan (in weeks) of individuals in each infection category. Because all hosts in the experiment were at least 7.65mm, these estimates were the survival rates for adult *E. depressus*, and we assumed that mortality rates were constant across all adult sizes (>6mm carapace width).

Many life history traits of ectotherms, such as survival, and reproduction rates, are expected to be zero at extreme temperatures and attain a maximum at an optimal temperature (25, 26). To evaluate the shape of the effect of temperature (T) on a given host or parasite performance trait, $R(T)$, we fit unimodal functions (Eq. S1-3 below) relating performance (i.e., lifespan and reproduction) to temperature with the R package *nls*, and used AICc model selection criteria to select the most parsimonious model. Specifically, to evaluate for evidence of no skew around the optimum value, we fit a quadratic function,

$$R(T) = c(T - T_{min})(T_{max} - T) \qquad \text{Eq. S1}$$

where T_{min} and T_{max} are the respective minimum and maximum temperatures at which performance is non-zero and c is a constant. Left-skewed temperature dependence (i.e. with a long left tail) was modeled using a Brière function (27):

$$R(T) = cT(T - T_{min})(T_{max} - T)^{\frac{1}{m}} \qquad \text{Eq. S2}$$

where *m* is a shape parameter determining the magnitude of the skew. Since the Brière function describes only left-skewed temperature dependence, we flipped and reversed it to create a modified Brière function that could fit a right-skewed pattern:

$$R(T) = c(-T + T_{min} + T_{max})(T_{max} - T)(T - T_{min})^{\frac{1}{m}} \quad \text{Eq. S3}$$

Because the package *nls* would not converge with the inclusion of the term 1/m, we ran sequential models for Eq. S2 and S3, varying 1/m, and then selected the model (and 1/m value) that minimized the AICc. We then compared and selected the best performing model between each fit (Eq. S1-3) using AICc, and we calculated T_{opt} using the *optimize* function in R.

iv. Supplemental results: At the end of the experiment there was 100% mortality of infected individuals for five of the temperature treatments (5º, 20º, 25º, 30º and 35ºC), 57% mortality at 15ºC, and 34% mortality at 10ºC (Fig S5). At the end of the experiment there was 100% mortality for the exposed (virgin externa) individuals at three of the temperatures (25º, 30º and 35º C), and a single individual was censored (i.e. removed prior to mortality) in the 5ºC treatment (Fig. S5). There was 50% mortality in the 20º C temperature treatment, 75% mortality in the 15º C temperature treatment and only 14% mortality in the 10ºC treatment (Fig. S5). For logistical reasons the susceptible host survival experiment was run for 159 days and there was 100% mortality in the extreme temperature treatments (5ºand 35º C), 92% mortality at 30ºC and only 16% mortality at 15ºC and no mortality at 20ºC (Fig. S5).

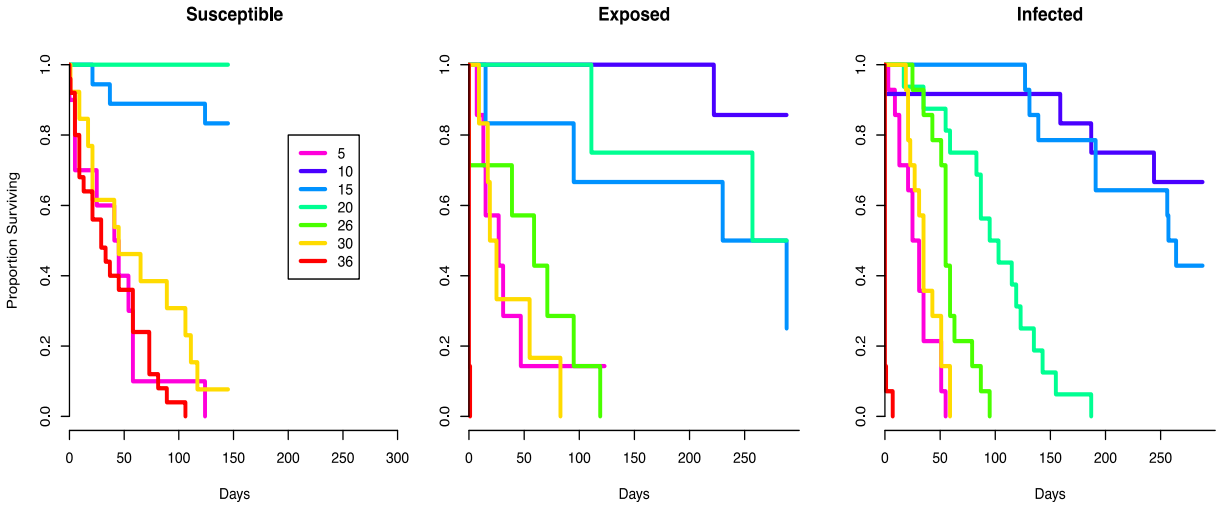

Figure S5. Kaplan-Meier survival analysis evaluating the effect of temperature on host survival for susceptible hosts (left), exposed hosts (middle) and infected hosts (right). Expected lifespan (used in the model) was evaluated by calculating the area under the curve for survival at each temperature.

Expected lifespan of susceptible hosts responded non-linearly to temperature and the best fitting function was a Brière function (Fig. 1, Table S2, Eq. S2). Expected lifespan of exposed and infected also responded non-linearly to temperature, and the best fitting function was a modified Brière (Fig. 1, Table S2, Eq. S3). Parasite reproduction also varied non-linearly with temperature and was best described by a modified Brière (Fig. 1, Table S2, Eq. S3).

Table S2. For each infection status and response variable, we report the best fit function, the estimated thermal minima (T_{min}), maxima (T_{max}) and thermal optima (T_{opt}) from that function, and the shape parameter (m) and scaling constant (c) for that function (Eq. S2 and S3). The difference in AICc score (ΔAICc) reports how much better the best fitting Brière or modified Briere function was over the quadratic model. More negative values suggest an increasingly better fit over the quadratic function. If data fit a Brière function then it did not fit a modified Brière function.

Infection status	Response	Function	T_{min}	T_{max}	T_{opt}	1/m	c	ΔAICc
Susceptible	Survival	Brière	3.14	34.80	18.26	2	0.00069	-8.96
Exposed	Survival	Modified Brière	4.95	34.44	10.24	0.4	0.03393	-9.31
Infected	Survival	Modified Brière	4.99	32.10	8.83	0.3	0.04414	-17.12
Infected	Reproduction	Modified Brière	9.88	30.75	15.9	0.65	0.0000003	-5.8

C. Modeling

***i. Model development and simplification*:** We investigated the ecological consequences of the thermal performance offset for host and parasite found in our experiments through a simple compartmental model. We used this model to describe seasonal disease dynamics in an *E. depressus* population within a single oyster reef, with open host recruitment and closed parasite recruitment (28). We modeled the host recruitment to an oyster reef as open, since the best available data suggest that crab larvae spend approximately 40 days in the plankton (8), opening great potential for mixing at the estuarine scale. We modeled parasite recruitment as closed because parasite larval duration is short (2-5 days) and it has been suggested that recruitment is maximized within 0.1 meters of release (29). Individuals within the host assemblage were categorized according to *L. panopaei* infection status, such that S represents the abundance of uninfected, susceptible *E. depressus*, E represents the abundance of *E. depressus* with internal infections, E_v represents the abundance of *E. depressus* with non-reproductive but visible infections (i.e., individuals with a virgin externa), and I represents infectious *E. depressus* (i.e., those with externa producing parasite larvae). Pelagic free-living infective stages of female and male parasite larvae are denoted by W_f and W_m respectively.

In the absence of the parasite, the adult crabs recruit to the local population at a seasonally varying rate $\Lambda(t)$ (described in Eq. S16 below), and experience per capita mortality at a rate μ_S. As crabs are not infectious below 6mm carapace width, recruitment here refers to the age class of crabs >6mm carapace width. When the parasite is introduced into the system, female parasite larvae colonize susceptible hosts at a rate C_f, and the host then becomes infected with probability π_f. Exposed hosts die at rate μ_E and move to the unmated virgin externa class at development rate τ. Virgin externa are colonized by male parasite larvae at rate C_m and become

infectious with probability π_m. Infectious host individuals die at rate μ_I, and release female and male parasite larvae at respective rates λ_f and λ_m. Pelagic larval mortality is considered equal (and high) for both sexes and occurs at rate μ_w. Therefore, parasite transmission can be described by the following system of equations:

$$\frac{dS}{dt} = \Delta - \mu_S S - \pi_f C_f W_f S \qquad \text{Eq. S4}$$

$$\frac{dE}{dt} = \pi_f C_f W_f S - \mu_E E - \tau E \qquad \text{Eq. S5}$$

$$\frac{dE_v}{dt} = \tau E - \mu_E E_v - \pi_m C_m W_m E_v \qquad \text{Eq. S6}$$

$$\frac{dI}{dt} = \pi_m C_m W_m E_v - \mu_I I \qquad \text{Eq. S7}$$

$$\frac{dW_f}{dt} = \lambda_f I - \mu_W W_f - C_f W_f S$$
$$\frac{dW_m}{dt} = \lambda_m I - \mu_W W_m - C_m W_m E_v \qquad \text{Eq. S8, S9}$$

Female parasite larvae must find a host, evade the host immune system and form an interna, whereas male larvae are left with the relatively simple task of fertilizing an infected host (which is presumably attempting to attract a mate; 30). As such, we assumed that male larvae were not the limiting factor for transmission (i.e., all exposed hosts that develop virgin externa are instantaneously mated and become infectious; $\pi_m C_m W_m E_v \approx \tau E$). Thus, we no longer consider the E_v and W_m classes, and all crabs surviving the latent period are assumed to enter the infectious class. Through this assumption we restrict the temperature limitation on the parasite to the female colonization rate – so that if the temperature is such that female larvae are being produced and colonizing then we assume that temperature will be acceptable for the male larvae colonization and externa development.

Since larval parasite mortality is high relative to host mortality (i.e., $\mu_w >> \mu_s$) and loss due to infection ($\mu_W >> C_f, C_m$), we can make a 'quasi-equilibrium' approximation by setting $\frac{dW_f}{dt}$ to zero, yielding:

$$W_f = \frac{\lambda_f I}{\mu_W} \qquad \text{Eq. S10}$$

Thus, the transmission rate in Eq. S5 can be written βSI, where β is the product of terms summarizing multiple components of host and parasite biology: the contact rate of parasite larvae with uninfected hosts, infection probability and the number of female larvae produced by one infectious host during the expected lifespan of a larva ($\frac{\lambda_f}{\mu_W}$) :

$$\beta = \frac{\pi_f c_f \lambda_f}{\mu_W} \quad \text{Eq. S11}$$

Under these assumptions, the model simplifies to:

$$\begin{aligned} \frac{dS}{dt} &= \Delta - \mu_S S - \beta SI \\ \frac{dE}{dt} &= \beta SI - \mu_E E - \tau E \\ \frac{dI}{dt} &= \tau E - \mu_I I \end{aligned} \quad \text{Eq. S12, S13, S14}$$

ii. Functional dependence in parameters on temperature and season: To explore how temperature affects host-parasite interactions we allowed several model parameters to vary with temperature, based on functional fits to the thermal performance curves generated from our experiments (Eq. S2-S3. Fig. 1A). Parasites in infectious hosts release larvae approximately once a week (16), so we ran our model at a weekly time step. To account for seasonal variability in temperature we used mean weekly temperatures from 2011-2014 collected by the Georgia Coastal Ecosystem (GCE) Long Term Ecological Research program (32-35; ambient; Fig. 3A). To best approximate the temperature experienced on a submerged oyster reef (the mud crab host's habitat), data was acquired from GCE station 10, a buoy located on a creek on Sapelo Island, GA at a depth of ~1m (approximately the depth of water found over an oyster reef in Georgia; 22, 31-34). We downloaded mean daily temperature and translated those to mean weekly temperatures averaged across 4 years, from 2011 to 2014. This level of averaging necessarily limits the maximum and minimum temperature experienced. However, the mean is relatively representative of the actual temperature experienced in this system because water temperature was fairly stable, with the daily standard deviation of water temperature between 0 and 1.7ºC for all four years (31-34). In addition, we obtained empirical estuarine temperature data ~150km north and south of our study site to allow for direct comparisons to our predictions from our central study site (35).

Model parameters were assumed to be a function of weekly water temperature, *T(t)*, or within year time (*t*). Temperature dependent model parameters (μ_S, μ_E, μ_I, and β) were updated weekly based on temperature. For each week of the model we updated the mortality rates and parasite reproductive rates by plugging the GCE temperature data into the Brière or modified Brière function for host/parasite response to temperature and updating the model (Fig. S6A).

The mortality rate for each class, $\mu_j(T)$ (j=*S,E,I*), is estimated as the inverse of the expected lifespan at each temperature *T* generated from the experiments (Fig. 1A). The shape of μ_S was described by a Brière function, Eq. S2, while the shape of μ_E, and μ_I were described by a modified Brière function, Eq. S3 (Table S3).

The transmission rate β is assumed to be proportional to the temperature dependent parasite reproduction rate (Fig. 1B) i.e .

$$\beta = bP(T) \quad \text{Eq. S15}$$

where the colonization probability *b* is a scaling constant (an agglomerate of the contact rate of female parasite larvae per susceptible host, the probability of successful parasite colonization, larval parasite longevity, and the fraction of female larvae produced; cf Eq. S11) determined by

matching model output to field estimates of seasonal infection prevalence at the study site (see section C.iii below for more details), and *P(T)* is the temperature-dependent parasite production rate fitted from experimental data (Eq. S3, Fig. 1B). It is possible that parasite colonization, longevity and infectivity, as well as host immunity, are also temperature-dependent. Because we have no data on these processes we make the simplifying assumption that any temperature dependence in transmission is primarily captured by the temperature dependence in larval parasite production.

Host recruitment rate, Δ, was set based on the number of *E. depressus* juveniles (<6mm carapace width) found per square meter in a survey conducted in 2010 (3). We accounted for potential seasonality in host recruitment by assuming that the weekly recruitment rate was a constant (*k*) or zero (Table S3). Thus, Δ =Δ(t) can be described as a step function, with recruitment at within year time t based on the phenology, *p*, of the middle of the recruitment period and the duration (*d*) of host recruitment:

$$\Delta(t) = \left\{ \begin{array}{ll} k, & p - \frac{d}{2} < t < p + \frac{d}{2} \\ 0, & otherwise \end{array} \right\} \qquad \text{Eq. S16}$$

While it seems plausible that the development rate from exposed to infectious stage, τ, could be temperature dependent, there is no evidence to support this relationship either in the literature or from our experiments. Therefore, we determined τ by tuning model output to field estimates of infection prevalence at the study site (see section C.iii., below). All model parameters used in the model simulations are summarized in Table S3.

Table S3. Description of model parameters, their dependence on temperature or time of year, and how they were estimated. Temperature dependent parameter estimates were updated weekly based on the best fit thermal performance curve (Eq. S1-3), seasonally dependent variables were regulated by a step function seasonally (Eq. S16), and constant parameters were held constant.

Term	Definition	Dependence	Notes
Δ	Host recruitment	Seasonal	constant weekly recruitment rate (*k*) estimated from literature (3), timing and duration of recruitment (*d*,*p*) estimated using field prevalence
μ_S	Susceptible host mortality	Temperature	Experiment (Fig. 1C)
μ_E	Exposed host mortality	Temperature	Experiment (Fig. 1D)
μ_I	Infected host mortality	Temperature	Experiment (Fig. 1E)
τ	Parasite development rate (exposed to infected)	Constant	0.05; Estimated from field prevalence
β	Transmission rate	Temperature	Assumed proportional to experimentally measured parasite reproduction rate (Fig. 1B); colonization probability (b) estimated using field prevalence

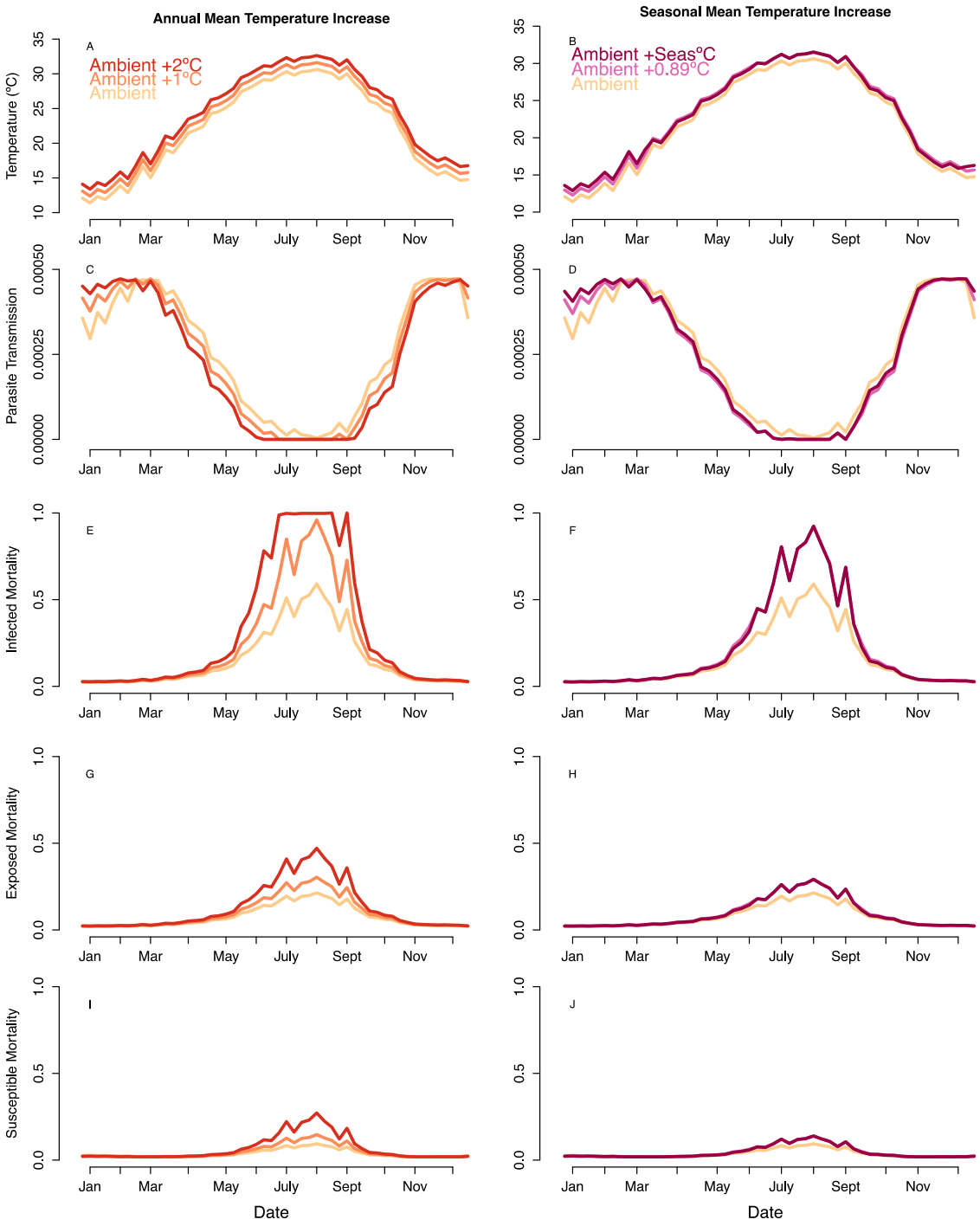

Figure S6. A) Temperatures used to drive seasonality in the host-parasite model, with the mean water temperature from the Georgia Coastal Ecosystem Long Term Ecological Research station 10 averaged weekly from 2011 to 2014 (peach), ambient +1ºC (orange), ambient +2ºC (red). B) Temperature increased based on historical temperature change in the southeast from 1970-2008 (36), with the ambient+0.89 ºC (pink) and seasonally varying increases (purple). Temperature dependent model parameters, including parasite transmission, β (C-D), infected host mortality (E-F), exposed host mortality (G-H) and susceptible host mortality (I-J).

iii. Parameter selection and sensitivity analysis*:* We did not have a priori published or experimental estimates of the timing and duration of host recruitment (*p* and *d* respectively), the development rate of the parasite in the host (i.e from initial colonization of the host to production of parasite larvae, τ), and the scaling constant *b* that relates experimentally measured parasite production rates to the transmission rate β. Therefore, we used field data on seasonal infection prevalence from 2010-2014 to determine the values of these parameters as follows. Each of these parameters was co-varied over a range of biologically plausible values: the timing of peak recruitment was assumed to lie between mid-May and late September (*p* = week 20 - week 38); the duration of recruitment *d* from 4-12 weeks; the parasite development rate τ from 0.04-0.33 (corresponding to a latent period of 3-25 weeks); and since the transmission constant incorporates multiple biological processes and was unknown to an order of magnitude, *b* was varied over a log scale (from 10^{-8} to 10^{-2}).

For each combination of the above 4 parameters, the model was run until dynamics settled into an annually repeating pattern (see section C.iv below for more details). For each week for which field prevalence estimates were available, we calculated infection prevalence from the model output, and calculated the sum of the squared difference between field and model prevalence. Parameter combinations were selected that minimized the sum squared difference between field and model prevalence. Since the best-performing parameter combinations resulted in similar sum square values, we report on a restricted range of parameters that gave the best fit for the data: peak recruitment occurred in early September (*p*= 34-36), the duration of recruitment, *d* = 4-6 weeks, the development rate τ = 0.04-0.06 (latent period of 16-25 weeks), and the parasite colonization probability parameter, *b* = 2-4 x 10^{-7}. We chose the model with the lowest sum of squares for the estimates for our tuned model parameters (*p*=34, *d*=6, τ=0.04 and *b*=4 x 10^{-7}). The performance of the top 50 combinations of these parameters, as well as the chosen parameterization for the climate change scenarios, is shown in Fig. S7.

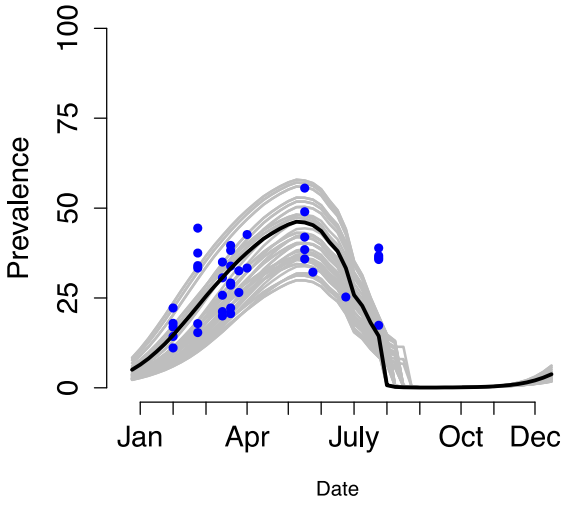

Figure S7. Model-predicted infection prevalence (grey lines) over an annual cycle for the 50 best parameter combinations that minimize the sum of squares distance from field infection prevalence data (blue circles). The black line depicts the parameter choice used in the main text to explore the climate change scenarios.

To understand how the choice of above parameterization influences the qualitative and quantitative dynamics of the model, we ran extensive sensitivity analyses by independently varying each of the above parameters, and co-varying the duration and timing of recruitment, over an extensive range and plotting the effect on the annual changes in infection prevalence (Fig. S8) and on the maximum, mean and minimum parasite prevalence and total host population size (Fig. S9). Recruitment duration and timing (*p*,*d*) influenced the timing, height and shape of the seasonal prevalence peak; however, all models predicted a drop in infection prevalence in the mid to late summer (Fig. S8A and B). Peak prevalence, but not its timing, was sensitive to changes in parasite colonization probability, *b* (Fig. S8D). However, with an order of magnitude increase in parasite colonization probability, there are modest changes in the maximum and mean prevalence relative to the baseline scenario, and the qualitative pattern is largely retained (Fig. S8D and Fig. S9B). Varying the parasite development rate τ influenced the maximum prevalence within a season, with peak prevalence reaching 100% when the latent period was short (i.e., 3 weeks or less; Fig. S8F). However, the pattern of seasonality in prevalence was robust to a wide range of estimates for the latent period from just under a month (3 weeks) to a little over six months (25 weeks; Fig. S8F).

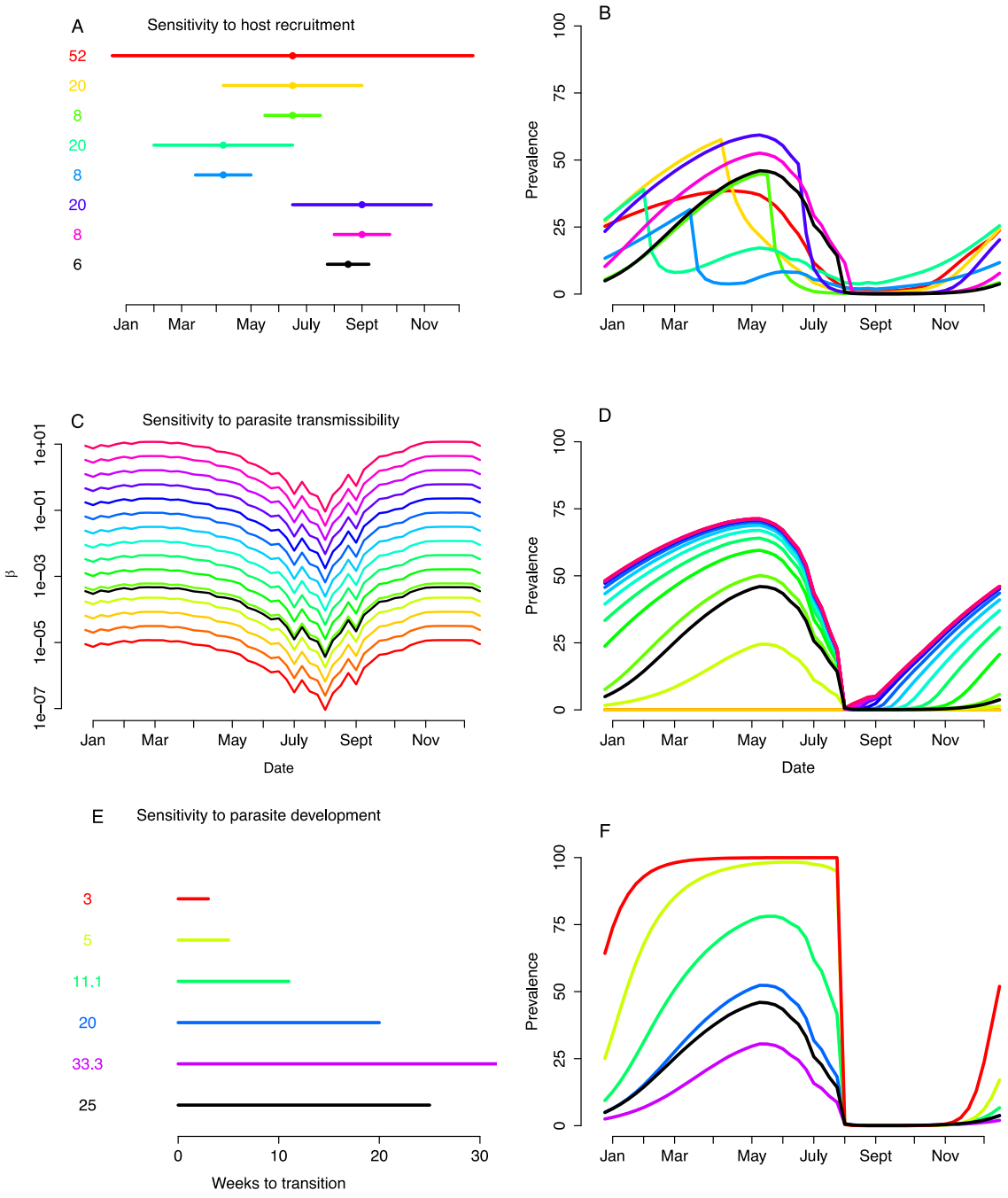

Figure S8. Sensitivity of modeled seasonal infection prevalence (right column, B,D,F) to respective changes in (A) host recruitment (co-variation of recruitment duration (d; width of lines) and timing (p; midpoint of lines), C) parasite transmissibility (β; with parasite colonization b, varied over a log scale from 10^{-8} to 10^{-2}), and E) parasite development (τ; line width represents corresponding duration of latent period=$1/\tau$). Black represents the parameter values (A, C, and E) and resulting model fit used in the manuscript (B, D, and F).

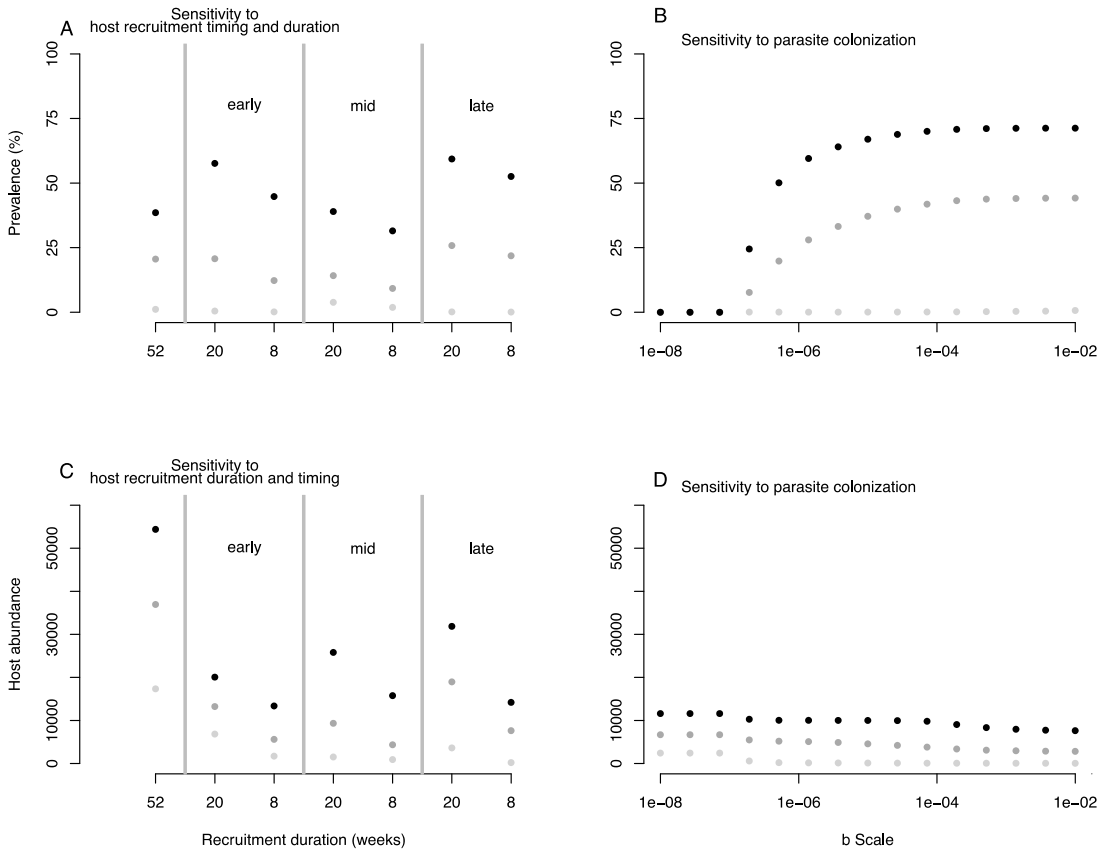

Figure S9. Maximum (black dots), mean (grey) and minimum (light grey) parasite prevalence (top row) and total host population size (bottom row) in response to changes in host recruitment duration and timing (A and C) and the constant relating parasite production to the parasite colonization probability, b (B and D). In A and C the vertical grey bars delineate variation in the timing of shorter-duration recruitment periods occurring with different seasonal timings of host larval recruitment (phenology, p): early (spring, week 16), mid (summer, week 26) and late (fall, week 36; Fig S8A). The duration of host recruitment, d, was run for a full year of recruitment (52 weeks) and at 20 and 8 weeks for each phenology. In B and D, parasite colonization probability scaled from 10^{-8} to 10^{-2}.

To quantitatively compare the relative sensitivity of model outcomes to parameter ranges, we independently varied the four fitted parameters (*d*,*p*,*b* and τ) around their values parameterized from field prevalence data, and recorded the absolute and % range of each parameter for which peak infection prevalence remained within +/- 20% of its modeled values, and its timing remained within 3 weeks of the modeled peak (i.e 17-25 weeks). The maximum magnitude and timing of prevalence was relatively robust to alterations in the timing of host recruitment with phenology (p), and parasite reproduction (b; Table S4). Maximum prevalence was relatively sensitive to changes in the duration of recruitment (d) and the parasite development rate within the host (τ, Table S4).

Table S4. Minimum and maximum absolute value (Min/Max value) and % variation (Min/Max % change) from set values in the main manuscript model (Set value) in model parameters that maintain reasonable model predictions of maximum prevalence (26-66%) and timing of maximum prevalence (17-25 weeks). Model parameters evaluated include host recruitment (p= timing of recruitment with phenology and d=duration of recruitment), parasite colonization probability (b), and the parasite development rate within the host (τ).

Parameter	Set value	Min % change	Min value	Max % change	Max value
p	6	-66	2.04	130	13.8
d	34	-25	24.5	30	44.2
b	1	-50	0.5	140	2.4
τ	25	-16	21	4	26

iv. Model simulations: Model simulations were run until a seasonally repeated pattern was reached. Patterns were considered annually repeating when the difference in infection prevalence for each week was less than 0.001% between years and the difference in weekly host abundance between years was less than one. Infection prevalence rapidly settled into a repeating within-year pattern, typically within 5 annual cycles (Fig. S10). Infection prevalence increased through the early months of the year, and began to rapidly decrease starting in week 23 (i.e. June; Fig. 2A). The initial decrease in prevalence is a result of a combination of decreasing parasite transmission and increasing infected mortality at warm summer temperatures (Fig. S6C and E). Infection prevalence continues to decline in late summer (August) due to the influx of recruiting susceptible hosts; continued warm water temperatures mean that parasite transmission remains low and infected host mortality is high (Fig. 2A, Fig. S6C and E).

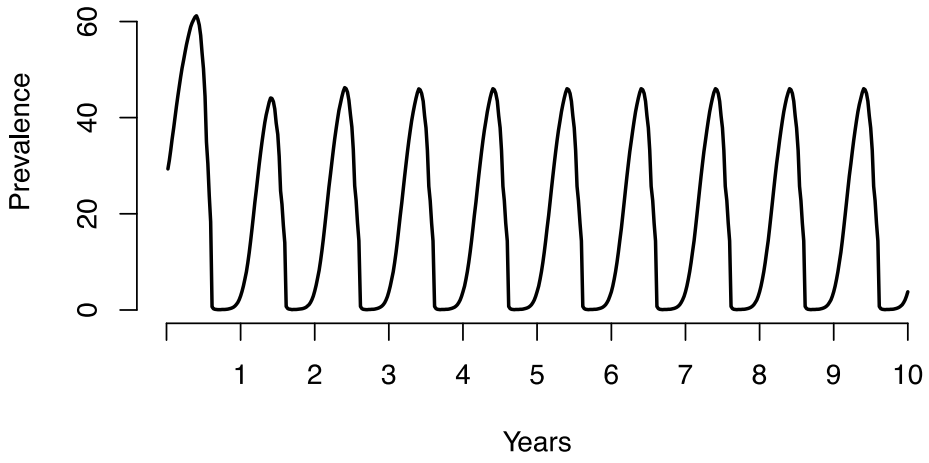

Figure S10. Seasonally varying prevalence over years, demonstrating the seasonally repeating pattern of infection prevalence after 5 annual cycles.

To understand how the presence of the parasite influenced seasonal host population dynamics, we ran a disease-free model in which seasonality was driven by seasonal host recruitment and the experimentally estimated susceptible host mortality rate (Fig. S11). Comparison of host population between the disease-free model and the model with infection reveals that the presence of infection within the model drives down the susceptible host abundance at all points in the year, but particularly in the spring and early summer; however, the timing of maximum and minimum host abundance remains relatively unchanged. Interestingly, the parasite reduced host abundance, even in the absence of direct effects of the parasite on crab recruitment (Fig. S11).

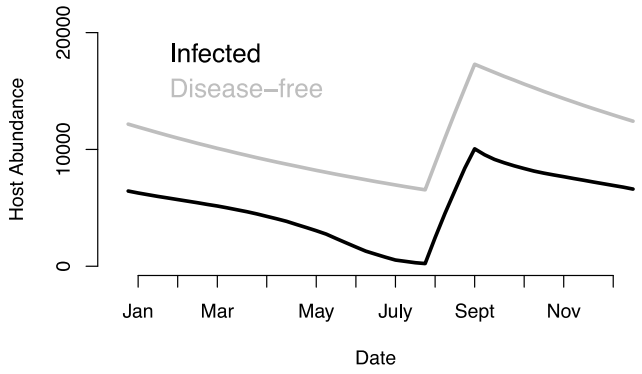

Figure S11. The total host abundance predicted in the disease-free model (grey) and the total host population (S, E and I) in the model run with infection.

v. ***Effect of coupling host recruitment with local parasite prevalence***

Because the parasite is castrating, it is possible that all reefs within the estuary are experiencing similar temperatures and epidemics, and thus that net host recruitment onto a focal reef could be reduced by parasitism. Accordingly, during the recruitment season we reduced the weekly recruitment rate in proportion to the abundance of exposed and infectious crabs 12 weeks prior (to account for larval and juvenile crab maturation). Thus, the expression for non-zero recruitment in equation (S16) is replaced by

$$\Delta(t) = k * \left(1 - \frac{E(t-12)+I(t-12)}{N(t-12)}\right) \qquad \text{Eq. S17}$$

When we modified host recruitment to account for a potential regional effect of castration of the infected hosts, the delay effect in the recruitment term caused the transient dynamics to last longer before prevalence settled into a repeating within-year pattern (approx. 100 years compared to <5 years for constant weekly recruitment). Parasite castration resulted in a reduced maximum host abundance, and consequently a lower peak in infection prevalence (Fig S12A and B). However, the seasonal pattern (i.e. the timing of maximum and minimum infection prevalence and host abundance) remained consistent between the two models (Fig. S12). Reduced prevalence under ambient temperatures meant that parasite extinction was even more likely under warming, namely a 1ºC rise in temperature extirpated the parasite in the model (Fig S12C).

In reality, the extent to which castration versus local density dependence or other biotic and abiotic factors (including temperature) limit host recruitment in this system is unknown. However, our simplifying assumption of constant weekly host recruitment within a seasonal window seems to represent a 'best-case' scenario for parasite persistence, with any additional forces that reduce host recruitment only more likely to reduce current parasite prevalence (Fig. S9B) or future persistence (Fig. S12C). Therefore, our conclusion of warming induced declines and extinction of the parasite in temperatures corresponding to the southeastern US is robust to different assumptions about host recruitment.

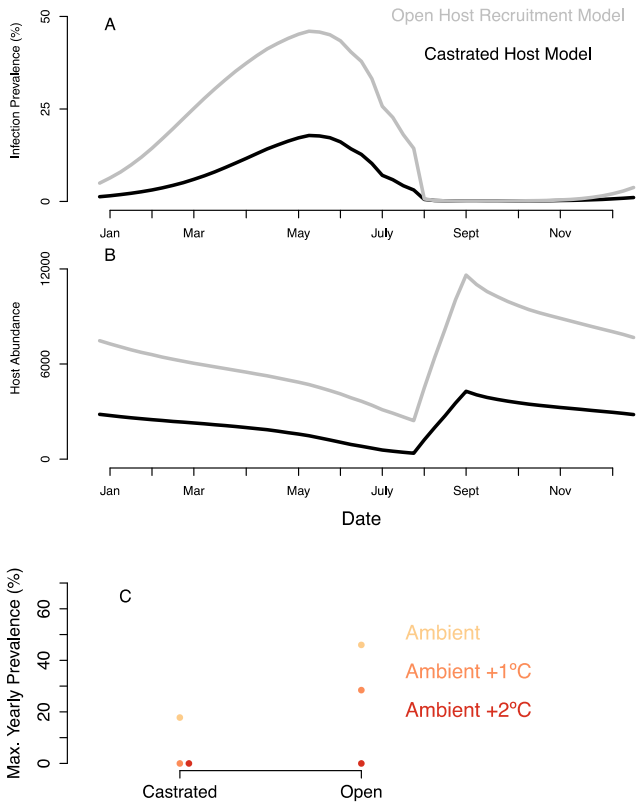

Figure S12. Model results with host recruitment (Δ) modified to account for castration of the host population (Castrated Host Model) compared to the results from the main manuscript model with host recruitment modeled as open (Open Host Recruitment Model). A) The infection prevalence predicted in the castrated host model (black) and the primary model with open host recruitment (grey). B) Total host population (S, E and I combined) in the castrated host model (black) and open host recruitment model (grey). C) Maximum yearly prevalence (%) predicted from model outputs run with weekly water temperature data from 2011-2014, a GCE-LTER mooring, GA for the castrated and open host recruitment models. We ran the model with ambient conditions (peach) and two warming scenarios, ambient +1ºC (orange), and ambient +2ºC (red). For the castrated host model, parasite prevalence for both ambient +1º and ambient +2º drops to zero, so we offset the +2ºC and +1ºC points for visibility.

vi. Temperature dependence and pathogen invasion potential

A useful summary measure of parasite invasion potential is the basic reproductive number, R_0 (37). If all rates in the model (Eq. S12-14) were constant through time, this expression would be

$$R_0 = \frac{\beta S^*}{\mu_I}\left(\frac{\tau}{\tau+\mu_E}\right) \qquad \text{Eq. S18}$$

where $S^* = \Delta/\mu_S$ is the disease-free equilibrium density.

In our system, the recruitment rate Δ is assumed to vary seasonally, but not with temperature, and the temperature dependence in the transmission rate β is assumed proportional to the temperature-dependent parasite production rate P. Therefore, at a constant temperature T, the temperature dependent pathogen reproductive number will be proportional to the temperature-sensitive traits estimated from the experiments as follows:

$$R_0(T) \propto \frac{P(T)}{\mu_I(T)\mu_S(T)}\left(\frac{\tau}{\tau+\mu_E(T)}\right) \qquad \text{Eq. S19}$$

The temperature-dependent R_0 (Eq. S19) shows a similar right-skewed response to temperature as the measured experimental parameters (exposed and infected host survival, parasite production, Figs. 1 B,D,E, and S13), with a T_{min}=9.88, T_{opt}=14.69 and T_{max}=30.75. Consistent with our model simulations, this suggests that warming that causes the host and parasite to experience an increased portion of the annual cycle at temperatures above the T_{opt} is likely to reduce infection prevalence. It also suggests that some cold-water sites where the parasite is currently excluded could become suitable for parasite invasion in the future (see section C.vii. below for more details).

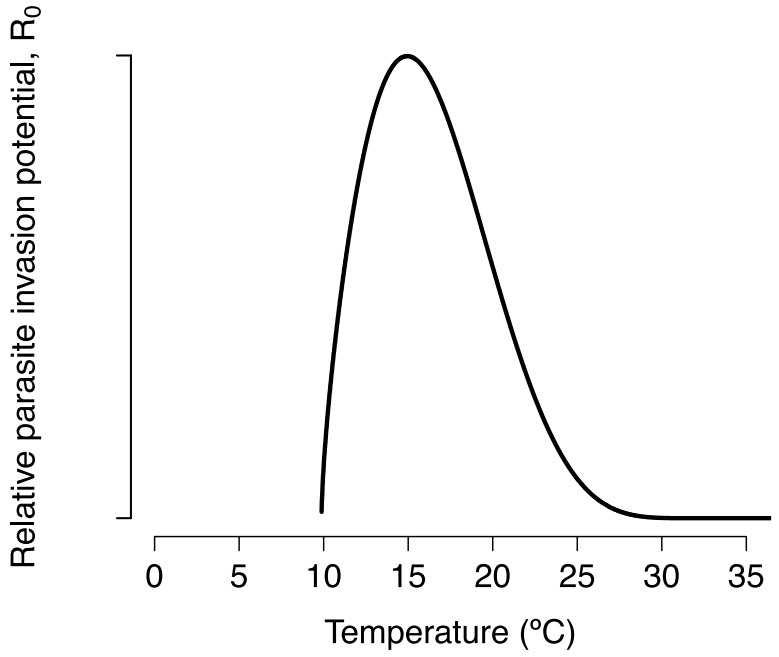

Figure S13. Temperature dependence in the thermal performance of R_0 (Eq. S19). Note that this is a relative R_0 because temperature-independent factors influence the scaling, such as seasonally varying host abundance (see Fig. S14).

Given the seasonal variation in recruitment that causes strong within-year variation in the availability of susceptible hosts, a more informative measure of the relative risk of parasite invasion through the annual cycle is to calculate an effective seasonal reproductive number. To do this we used estimates of thermal performance traits at each weekly mean temperature, T_w in week w, multiplied by the host population size in week w in the absence of the pathogen, $S(T_w)$ (calculated by running the disease-free model with seasonally varying recruitment and temperature-dependent susceptible mortality; Fig. S11):

$$R_0(T_w) = \frac{bP(T_w)S(T_w)}{\mu_I(T_w)}\left(\frac{\tau}{\tau+\mu_E(T_w)}\right) \quad \text{Eq. S20}$$

Consistent with the model output, calculating the seasonally varying effective reproductive number R_0 revealed that pathogen invasion potential peaks in late fall and winter following the fall recruitment pulse, and drops below the threshold value of one in the summer months (Fig. S14). Additionally, all warming scenarios predict an increase in the number of weeks for which the effective reproductive number drops below one.

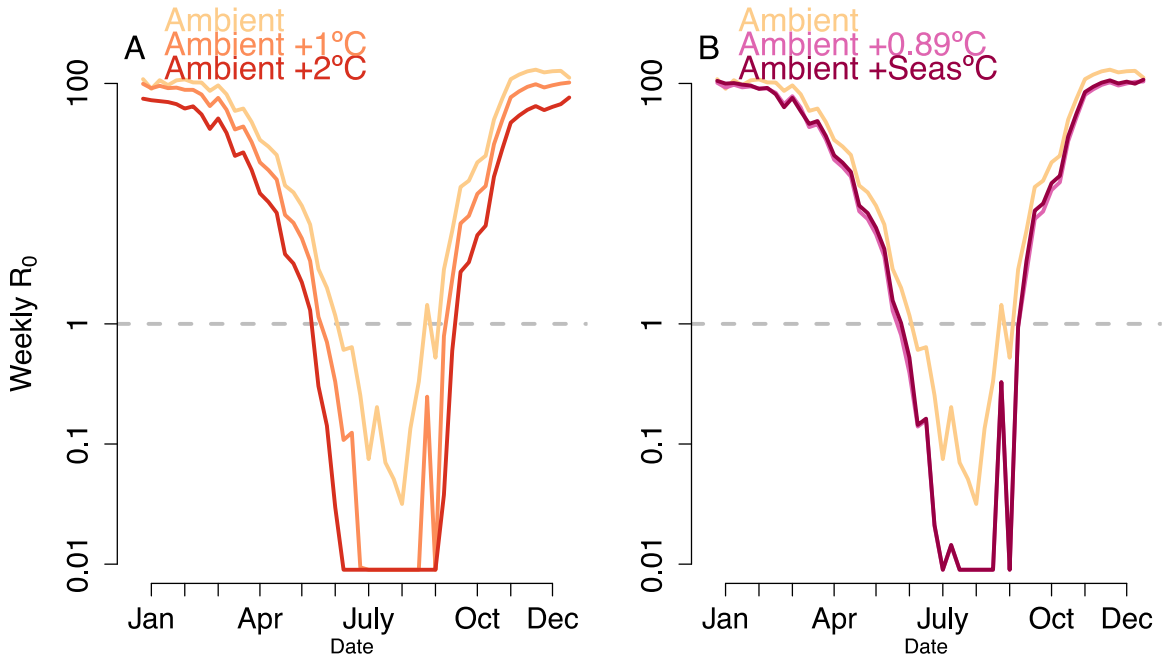

Figure S14. Seasonal varying effective reproductive number, R_0, estimated from model parameters at within year date d, and mean water temperature T_d (Eq. S20). The grey dashed line indicates where R_0=1, the minimum level needed for a parasite to invade a population. A) R_0 estimated with mean water temperature from the Georgia Coastal Ecosystem Long Term Ecological Research station 10 averaged weekly from 2011 to 2014 (peach), ambient +1ºC (orange), ambient +2ºC (red). B) R_0 estimated with mean water temperature increased based on historical temperature change in the southeast from 1970-2008 (36), with the ambient+0.89 ºC (pink) and seasonally varying increases (purple).

vii. Potential for northern parasite range expansion

Our modeling results predict general declines in prevalence and a range contraction of the parasite in the southern part of the host and parasite range. Since the timing and duration of host recruitment may be quite different in the northern part of the host range, accurate predictions of infection dynamics would require re-estimation of host recruitment parameters based on seasonal host abundance in this region. Nonetheless, we can estimate whether temperate change at more northerly latitudes will be more or less conducive to parasite transmission by focusing on temperature-induced changes to host survival by infection status, and parasite production, using Eq. S19 for thermal dependence in R_0. To do this, we evaluated the number of weeks in the year for which local weekly mean temperatures are likely conducive to parasite transmission potential. We included temperature values associated with R_0 values that were above the 25th quantile of all temperature dependent R_0 values (9.91-25.56ºC; Fig. S15) at each of 7 locations spanning the host's Atlantic coast range. We used mean weekly temperatures from National Estuarine Research Reserve creek monitoring locations averaged across 2011-2014 (Table S5; 35). If a given week within a year was missing data, then we averaged across the available number of years. The furthest north creek site (RI) had missing data in January, February and

early March for all years, because ice in the creek inhibited monitoring (38). We filled in the missing weeks with data from a nearby wharf monitoring system where access was not inhibited by ice (NERR station code: nartbwq). We then calculated the change in the number of weeks with temperatures conducive to parasite transmission under ambient, +1º, and +2ºC temperature conditions for all sites.

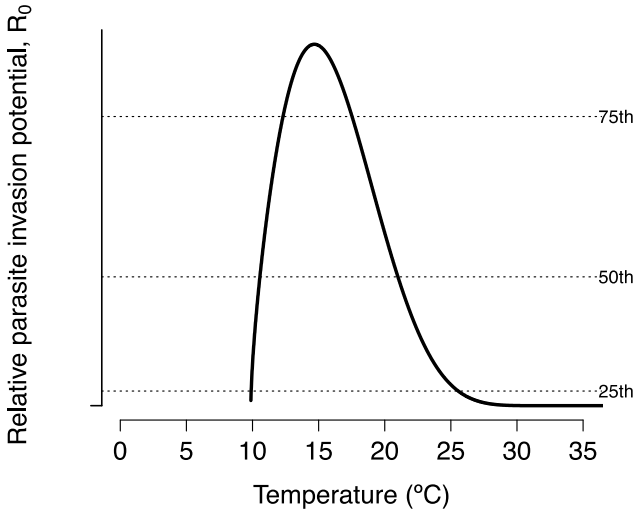

Figure S15. Temperature dependent R_0 (Fig. S13) with the dashed lines indicating the 25th, 50th and 75th quantile. The temperatures associated with the 25th quantile of R_0 (9.91 - 25.56ºC) were used to delineate temperatures likely conducive for parasite transmission.

Table S5. The state, location and National Estuarine Research Reserve stations label whose temperature data were used to calculate the ambient weekly mean temperature (2011-2014; 35).

State	State abbreviation	NERR Station Code	Latitude	Longitude
Rhode Island	RI	narncwq	41.62485	71.324283
New Jersey	NJ	jacb6wq	39.5079	74.3385
Virginia	VA	cbvtcwq	37.414986	76.71442
North Carolina	NC	nocrcwq	34.156	77.8499
South Carolina	SC	acefcwq	32.6358	80.3655
Florida	FL	gtmpcwq	29.667071	81.257403

Consistent with our model simulations, we found that there was a decrease in the number of weeks with temperatures conducive to transmission at sites in Florida, Georgia and South Carolina, with the greatest decrease at the southernmost location (Fig. S16). Interestingly, we also found that there was a decrease in the number of weeks with temperatures conducive to parasite transmission in Rhode Island, north of the parasite's current published northern limit (Fig. S16). At this furthest north site the 2ºC increase in winter temperatures only slightly increased the number of weeks with temperature conducive to parasite transmission, while the increased summer temperatures lead to a greater decrease in the number of weeks with

conducive temperatures (Fig. S17). We found that for three sites within the middle of the parasite's current range (North Carolina, Virginia and New Jersey; Fig. S16), the number of weeks with temperature conducive to parasite transmission will increase under 1º and 2ºC warming. Together, this suggests that under warming we could expect the parasite's range to contract in the south, with no northward expansion, but with the potential for local increases in transmission in the northern portion of the parasite's current range. It should be cautioned that these projections assume no local adaptation of thermal tolerance along this gradient, and assumes even temperature change throughout the season. Thus, this analysis highlights areas where further work measuring host and parasite thermal performance could be particularly beneficial for predicting changes in infection prevalence and range shifts for *L. panopaei.*

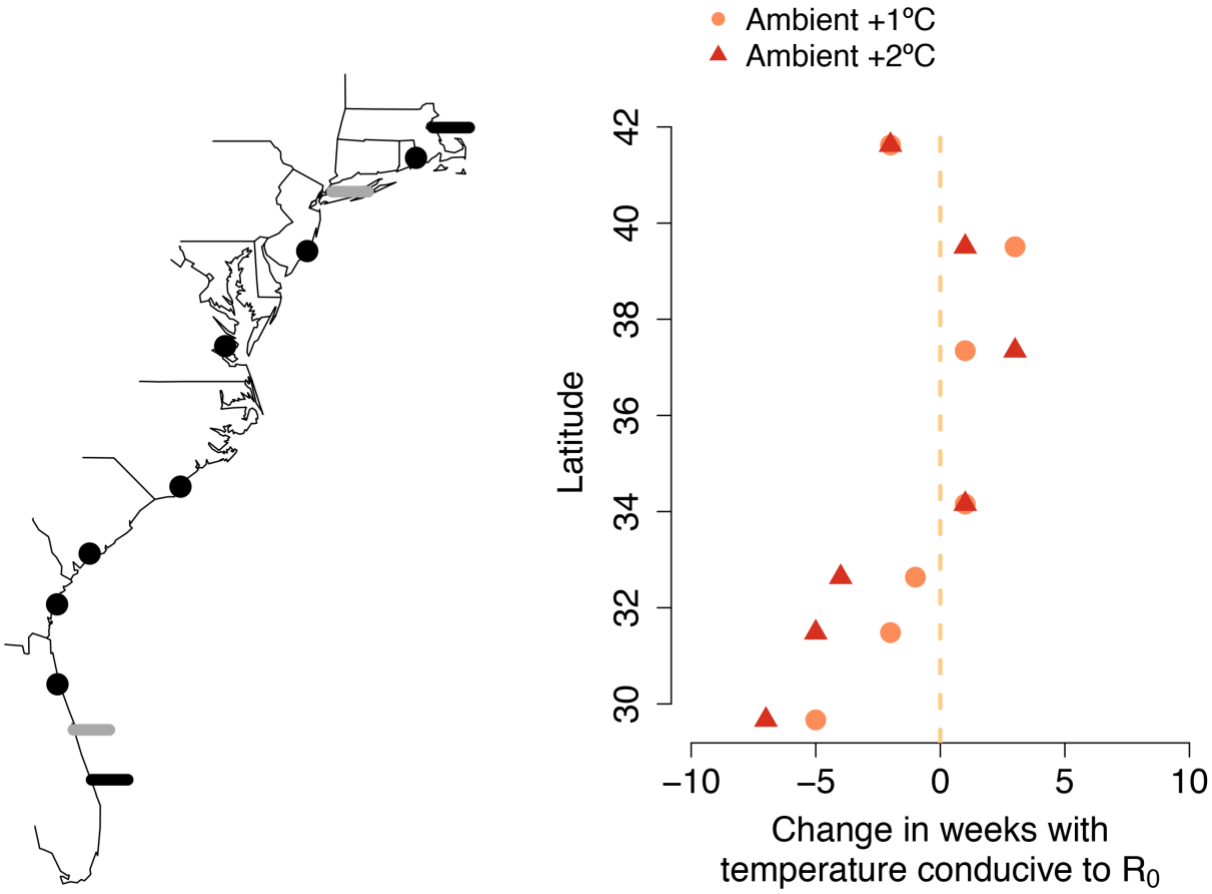

Figure S16. The change in number of weeks conducive to parasite transmission, i.e. weeks whose mean temperatures are in the range for which R_0 values were above the 25th quantile of all temperature dependent R_0 values (Fig. S15; 9.91 - 25.56ºC), under ambient +1ºC and ambient +2ºC warming, at 7 locations spanning the host's latitudinal range along the Atlantic coast (black dots on map; Table S5). Sites with a negative change (left of the peach dashed line) are predicted to have a decrease in transmission and those with a positive change could experience increased transmission. The recorded northern and southern limit on the east coast of the United States of the host (black lines) and parasite (grey lines) are indicated on the map (12, 39, 40). It should be noted that the native range of *L. panopaei* is in the Gulf of Mexico and is not considered in this analysis.

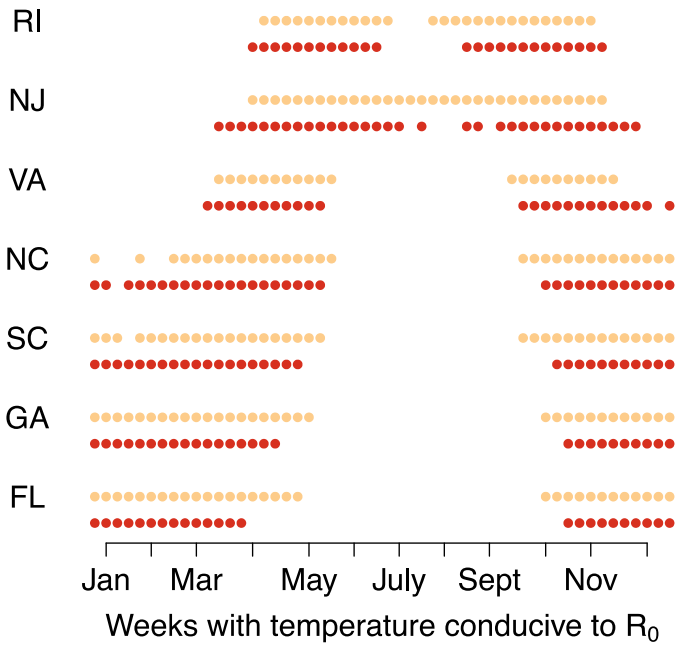

Figure S17. The number of weeks with temperatures conducive to parasite transmission under ambient (peach) and ambient +2ºC (red) temperatures at seven sites along the Atlantic coast (Table S5).

References:

1. Hulathduwa YD, Stickle WB, Brown KM (2007) The effect of salinity on survival, bioenergetics and predation risk in the mud crabs *Panopeus simpsoni* and *Eurypanopeus depressus*. *Mar Biol* 152(2):363–370.

2. Grant J, McDonald J (1979) Desiccation tolerance of *Eurypanopeus depressus* (smith)(Decapoda: Xanthidae) and the exploitation of microhabitat. *Estuaries Coast* 2(3):172–177.

3. Gehman A-LM, et al. (2017) Predators, environment and host characteristics influence the probability of infection by an invasive castrating parasite. *Oecologia*:139–149.

4. McDonald J (1982) Divergent life history patterns in co-occuring intertidal crabs *Panopeus herbstii* and *Eurypanopeus depressus* (Crustacea: Brachyura: Xanthidae). *Mar Ecol Prog Ser* 8:173–180.

5. Tolley SG, et al. (2006) Impacts of salinity and freshwater inflow on oyster-reef

communities in Southwest Florida. *Aquat Living Resour* 19(4):371–387.

6. Jones MB, Epifanio CE (1995) Settlement of brachyuran megalopae in Delaware Bay: an analysis of time series data. *Mar Eco Prog Ser* 125:67–76.

7. Costlow J, Bookhout C (1961) The Larval Development of *Eurypanopeus Depressus* (Smith) Under Laboratory Conditions). *Crustaceana* 2(1):6–15.

8. Mirkes DZ, Vernberg WB, DeCoursey PJ (1978) Effects of cadmium and mercury on the behavioral responses and development of *Eurypanopeus depressus* larvae. *Mar Biol*. 47:143-147.

9. Sulkin SD, Van Heukelem W, Kelly P (1983) Behavioral basis of depth regulation in hatching and post-larval stages of the mud crab *Eurypanopeus depressus*. *Mar Ecol Prog Ser* 11:157–164.

10. Epifanio CE, Tilburg C (2008) Transport of blue crab larvae in the Middle Atlantic Bight: A wet and windy journey. *J Mar Res* 66(6):723–749.

11. Kruse HH, Hare MP, Hines AH (2011) Genetic relationships of the marine invasive crab parasite *Loxothylacus panopaei*: an analysis of DNA sequence variation, host specificity, and distributional range. *Biol Invasions* 14(3):701–715.

12. Kruse HH, Hare MP (2007) Genetic diversity and expanding nonindigenous range of the rhizocephalan *Loxothylacus panopaei* parasitizing mud crabs in the western north Atlantic. *J Parasitol* 93(3):575–582.

13. Eash-Loucks WE, Kimball ME, Petrinec KM (2014) Long-term changes in an estuarine mud crab community: evaluating the impact of non-native species. *J Crustacean Biol* 34(6):731–738.

14. O'Shaughnessy KA, Harding JM, Burge EJ (2014) Ecological effects of the invasive parasite *Loxothylacus panopaei* on the flatback mud crab *Eurypanopeus depressus* with implications for estuarine communities. *Bull Mar Sci* 90(2):611–621.

15. Walker G (2001) Introduction to the Rhizocephala (Crustacea: Cirripedia). *J Morphol* 249(1):1–8.

16. Walker G, Clare A, Rittschof D, Mensching D (1992) Aspects of the life-cycle of *Loxothylacus panopaei* (Gissler), a sacculinid parasite of the mud crab *Rhithropanopeus harrisii* (Gould): a laboratory study. *J Exp Mar Biol Ecol* 157(2):181–193.

17. Glenner H (2001) Cypris metamorphosis, injection and earliest internal development of the Rhizocephalan *Loxothylacus panopaei* (Gissler). Crustacea: Cirripedia: Rhizocephala: Sacculinidae. *J Morphol* 249:43–75.

18. Alvarez F, Hines AH, Reaka-Kudla M (1995) The effects of parasitism by the

barnacle *Loxothylacus panopaei* (Gissler)(Cirripedia: Rhizocephala) on growth and survival of the host crab *Rhithropanopeus harrisii* (Gould)(Brachyura: Xanthidae). *J Exp Mar Biol Ecol* 192:221–232.

19. Hoeg JT (1995) The biology and life cycle of the rhizocephala (Cirripedia). *J Mar Biol Ass UK* 75:517–550.

20. Alvarez F (1993) The interaction between a parasitic barnacle *Loxothylacus panopaei* (Cirripedia, Rhizocephala) and three of its host crab species (Brachyura, Xanthidae) along the East coast of North America. University of Maryland.

21. Kimbro DL, Byers JE, Grabowski JH, Hughes AR, Piehler MF (2014) The biogeography of trophic cascades on US oyster reefs. *Ecol Lett* 17(7):845–854.

22. Byers JE, et al. (2015) Geographic variation in intertidal oyster reef properties and the influence of tidal prism. *Limnol Oceangr* 60(3):1051–1063.

23. R Development Core Team (2017) R: A language and environment for statistical computing. Available at: http://www.R-project.org/.

24. Royston P, Parmar MKB (2013) Restricted mean survival time: an alternative to the hazard ratio for the design and analysis of randomized trials with a time-to-event outcome. *BMC Med Res Methodol* 13(1):152.

25. Dell AI, Pawar S, Savage VM (2011) Systematic variation in the temperature dependence of physiological and ecological traits. *Proc Natl Acad Sci* 108(26):10591–10596.

26. Amarasekare P, Sifuentes R (2012) Elucidating the temperature response of survivorship in insects. *Funct Ecol* 26(4):959–968.

27. Briere J-F, Pracros P, Roux A-YL, Pierre J-S (1999) A novel rate model of temperature-dependent development for Arthropods. *Environ Entomol* 28(1):22–29.

28. Kuris AM, Lafferty KD (1992) Modelling crustacean fisheries: effects of parasites on management strategies. *Can J Fish Aquat Sci* 49(2):327–336.

29. Grosholz ED, Ruiz G (1995) Does spatial heterogeneity and genetic variation in populations of the xanthid crab Rhithropanopeus harrisii (Gould) influence the prevalence of an introduced parasitic castrator? *J Exp Mar Biol Ecol* 187(1):129–145.

30. Ritchie L, Høeg J (1981) The life history of Lernaeodiscus porcellanae (Cirripedia: Rhizocephala) and co-evolution with its porcellanid host. *J Crustacean Biol* 1(3):334–347.

31. Di Iorio D (2012) Continuous salinity, temperature and depth measurements from moored hydrographic data loggers deployed at GCE10_Hydro (Duplin River west of

Sapelo Island, Georgia) from 01-Jan-2011 through 31-Dec-2011. doi:http://dx.doi.org/10.6073/pasta/c705a3cf1492716c7ac19d7cd1423b55.

32. Di Iorio D (2013) Continuous salinity, temperature and depth measurements from moored hydrographic data loggers deployed at GCE10_Hydro (Duplin River west of Sapelo Island, Georgia) from 01-Jan-2012 through 31-Dec-2012. doi:http://dx.doi.org/10.6073/pasta/73b48d6008a86509291b97e513307b85.

33. Di Iorio D (2014) Continuous salinity, temperature and depth measurements from moored hydrographic data loggers deployed at GCE10_Hydro (Duplin River west of Sapelo Island, Georgia) from 01-Jan-2013 through 31-Dec-2013. doi:http://dx.doi.org/10.6073/pasta/9f24a43f1d02b3f80c9cff2dfc9e33e5.

34. Di Iorio D (2014) Continuous salinity, temperature and depth measurements from moored hydrographic data loggers deployed at GCE10_Hydro (Duplin River west of Sapelo Island, Georgia) from 01-Jan-2014 through 31-Dec-2014. doi:http://dx.doi.org/10.6073/pasta/1b0236a552de365151163eb530299469

35. NOAA National Estuarine Research Reserve System (NERRS). System-Wide Monitoring Program. Data accessed from the NOAA NERRS Centralized Data Management Office website: http://www.nerrsdata.org/; accessed 2017.

36. Karl T, Melillo J, Peterson T (2009) *Global climate change impacts in the United States* (Cambridge University Press).

37. Keeling MJ, Rohani P (2008) *Modeling infectious diseases in humans and animals*. (Princeton University Press).

38. Durant D, Raposa KB (2011) *Water quality, nutrients and meteorological trends at the Narragansett Bay National Estuarine Research Reserve in 2009*.

39. Freeman AS, Blakeslee AMH, Fowler AE (2013) Northward expansion of the rhizocephalan Loxothylacus panopaei (Gissler, 1884) in the northwest Atlantic. *Aquat Invasions* 8(3):347–353.

40. Williams AB (1984) *Shrimps, lobsters, and crustaceans of the atlantic coast of the eastern United States, Maine to Florida* (Smithsonian Institution Press, Washington, D.C.).